1st International Conference on Experiments/Process/System Modelling/Simulation/Optimization
1st IC-EpsMsO
Athens, 6-9 July, 2005

HYBRID GAS BEARINGS FOR OIL-FREE TURBOMACHINERY: EXPERIMENTS AND MODEL VALIDATION

Luis San Andrés

Turbomachinery Laboratory, Mechanical Engineering Department
Texas A&M University
College Station, TX 77843-3123, USA
e-mail: lsanandres@mengr.tamu.edu, web page: http://phn.tamu.edu/TRIBGRoup

Keywords: Gas Bearings, Rotordynamics, Oil-Free Turbomachinery

Abstract. *Gas film bearings offer unique advantages enabling successful deployment of high-speed micro-turbomachinery. Current applications encompass micro power generators, air cycle machines and turbo expanders. Mechanically complex gas foil bearings are in use; however, their excessive cost and lack of calibrated predictive tools deter their application to mass-produced oil-free turbochargers, for example. The present investigation advances the analysis and experimental validation of hybrid gas bearings with static and dynamic force characteristics desirable in high-speed turbomachinery. These characteristics are adequate load support, good stiffness and damping coefficients, low friction and wear during rotor startup and shutdown, and most importantly, enhanced rotordynamic stability at the operating speed. Hybrid (hydrostatic/hydrodynamic) flexure pivot-tilting pad bearings (FPTPBs) demonstrate superior static and dynamic forced performance than other geometries as measured in a high speed rotor-bearing test rig operating to a top speed of 100 krpm. A computational model including the effects of external pressurization predicts the rotordynamic coefficients of the test bearings and shows good correlation with measured force coefficients, thus lending credence to the predictive model. In general, direct stiffnesses increase with operating speed and external pressurization; while damping coefficients show an opposite behavior.*

1. INTRODUCTION

Micro-turbomachinery demands gas bearings to ensure compactness, lightweight and extreme temperature operation. Gas bearings with large stiffness and damping, and preferably of low cost, will enable successful commercial applications. Current applications encompass micro power generators, air cycle machines and turbo expanders. Mechanically complex gas foil bearings are in use; however, their excessive cost and lack of calibrated predictive tools deter their application to mass-produced oil-free turbochargers, for example.

Gas film bearings, unlike oil-lubricated bearings, offer advantages of low friction and less heat generation. These advantages enable their successful applications in air-cycle units for airplanes, high-precision instruments, auxiliary power units, and high-speed micro-turbomachinery. In addition, gas bearing systems do not require costly, complex sealing and lubricant circulation systems. Furthermore, these oil-free bearing applications eliminate process fluid contamination and are environmental friendly.

Our main objective is to advance the technology of gas film bearings for applications to oil-free turbomachinery by demonstrating their rotordynamic performance, reliability and durability. References [1-4] detail the research progress to date. Wilde and San Andrés[1,2] describe rotordynamic measurements and analyses conducted on a small rotor supported on three lobed hybrid gas bearings. For various imbalance conditions, coast down tests from 60,000 rpm characterize the rotor response supported on the bearings. As the supply pressure rises, the rotor response shows an increase in critical speed and a noticeable reduction in damping ratio. Threshold speeds of instability also increase with increasing supply pressures, and whirl frequency ratios range from nearly 50% of rotor speed for a purely hydrodynamic condition to 25 % for a pressure supply five times ambient.

Zhu and San Andrés[3] investigate the dynamic forced performance of the same test rotor supported on hybrid flexure pivot - tilting pad bearings (FPTPBs). The bearings demonstrate stable performance and ability to carry dynamic loads up to 99 krpm (limit of the drive motor). Although the FPTPBs are mechanically complex and costlier than cylindrical plain bearings, their enhanced stability characteristics and predictable rotordynamic

performance are desirable for high speed turbomachinery applications. Experimental rotor responses show that feed pressure increases the bearings' direct stiffness and critical speed while the viscous damping ratio decreases. Predictions correlate favorably with experimentally identified synchronous direct stiffness, though test damping force coefficients are smaller. Tests without feed pressure show the rotor becomes unstable at ~ 81 krpm with a whirl frequency ratio of 20%. The instability caused the rotor to rub and burn its protective Teflon coating.

Gas bearings, however, have a very low load carrying capacity and require of minute film thickness to accomplish their intended function. Thus, their fabrication and installation tends to be expensive and time consuming. Other disadvantages include little damping because of the gas inherently low viscosity. The provision of pressurized gas during start-up and shutdown periods is desirable to avoid transient rubs and reduce wear. A hybrid bearing configuration offers the combination of hydrostatic and hydrodynamic effects on the bearing static and dynamic forced performance. External pressurization provides additional direct stiffness for operation at all rotor speeds and reduces the journal eccentricity. Thus, a hybrid mode operation ultimately results in reduced power consumption. Incidentally, infamous disadvantages stem from two types of instabilities: pneumatic hammer controlled by the flow versus pressure lag in the pressurized gas feeding system, and hydrodynamic instability, a self-excited motion characterized by subsynchronous (forward) whirl motions[5, 6]. A properly designed hybrid bearing system aids to minimize these two kinds of instabilities.

Tilting pad bearings can eliminate the typically harmful hydrodynamic instability by not generating cross-coupled stiffness coefficients. Critical turbomachinery operating well above its critical speeds is customarily implemented with tilting pad bearings. Note that the multiplicity of parameters associated with a tilting pad bearing demands complex analytical methods for predictions of force coefficients and stability calculations [6, 7]. Although tilting pad bearings are not prone to induce subsynchronous instabilities; their time-accumulating drawbacks, namely pad wear and flutter and loss of nominal clearance, result in poor performance in the long run. The flexure pivot – tilting pad bearing (FPTPB) offers a marked improvement over the conventional design since its wire EDM construction renders an integral pads-bearing configuration, thus eliminating pivot wear and stack up of tolerances on assembly. Reference[8] describes the EDM process to fabricate this bearing type, with successful industrial applications given in[9, 10] and demonstrating FPTPBs have a larger load capacity and lower lubricant temperature raise than conventional tilting pad bearings.

Predictive models for liquid lubricated FPTPBs are well known[11, 12]. Czolczynsk[13] provides a comprehensive review of gas bearing applications and the numerical analysis for prediction of frequency dependent force coefficients. San Andrés and students[14, 15] advance finite element and finite difference analyses of gas bearings with numerically stable algorithms for accurate dynamic force performance prediction into very high speeds and minute clearances.

This paper presents a computational analysis predicting the dynamic forced performance of FPTPBs supplied with pressurized air, i.e. a hybrid bearing configuration. In a high speed test ring, rotor displacements and bearing transmitted forces are measured during coast-down tests, and the bearings' stiffness and damping coefficients are estimated from the recorded displacements and forces. Predicted stiffness and damping coefficients are in close agreement with the identified bearing coefficients.

2. ANALYSIS OF HYDROSTATIC/HYDRODYNAMIC GAS FILM BEARING

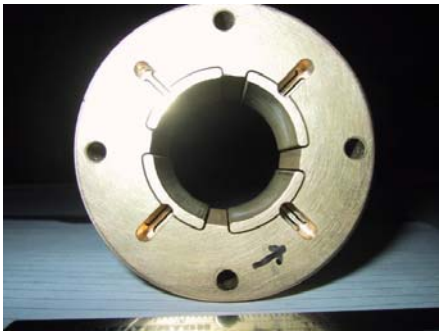

Figure 1. Flexure pivot tilting pad–gas bearing for oil-free test rig

Figure 1 shows a flexure pivot-tilting pad gas bearing, a one-piece mechanical component EDM fabricated. Figure 2 depicts a schematic view of a tilting pad with its relevant nomenclature. Each pad connects to the bearing through a thin flexural web, which provides a low rotational stiffness, thus ensuring small cross-coupled stiffnesses and avoiding subsynchronous instabilities into very high speed operation. For operation with external pressurization, a feed orifice is machined through the thin web.

The journal rotates at speed (Ω) and $\left(e_X, e_Y\right)$ denote the journal displacements within the bearing clearance. The film thickness (h) is described relative to the coordinate system ($x=R\cdot\theta$, y). Each pad extends from Θ_l to Θ_t (leading and trailing edge angular coordinates) with three degrees of freedom corresponding to angular (tilt) rotation (δ_p), radial (ξ_p)

and transverse displacements (η_p). The support web, modeled as an elastic structure with viscous type damping, provides reaction moments (M_P) and forces (F_ξ, F_η)$_P$. The film thickness on a pad is

$$h = C_p + e_X \cos\theta + e_Y \sin\theta + (\xi_p - r_p)\cos(\theta - \Theta_p) + (\eta_p - R\delta_p)\sin(\theta - \Theta_p) \quad (1)$$

where C_P and r_p are the nominal clearance and pad preload at the offset Θ_P angle where the elastic web is attached.

In an ideal gas undergoing an isothermal process, the density and pressure are related by $\rho = \dfrac{P}{\Re_g \cdot T}$, with $\Re_g$ and T representing the gas constant and operating temperature, respectively. The Reynolds equation for an ideal gas describes the inertialess and isoviscous flow within the thin film. This equation establishes the balance of pressure and shear driven mass flow rates and the mass flow rate ($\dot{m}_{OR}$) from an external pressure source, i.e.

$$\nabla \cdot \left(\frac{-h^3 P}{12\mu} \cdot \nabla(P) \right) + \frac{\Omega \cdot R}{2} \cdot \frac{\partial}{\partial x}(Ph) + \frac{\partial}{\partial t}(Ph) = 0 \quad (2)$$

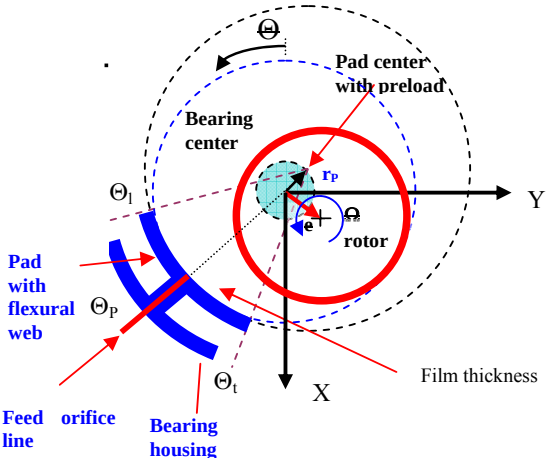

Figure 2. Geometry of a flexure-pivot pad with orifice for external pressurization

The pressure is ambient (P_a) on the sides (z=0, L) of a bearing pad, The orifice mass flow rate, $\dot{m}_{OR}$, depends on the pressure ratio $\overline{P} = P_{or}/P_s$ the orifice diameter (d) and the local film thickness (h), i.e. [16]

$$\dot{m}_{OR} = \pi\, d\, h\, \frac{P_s}{\sqrt{\Re_g T}} \cdot \Phi(\overline{P}) \quad (3)$$

with

$$\Phi_{(\overline{P})} = \begin{cases} \left(2 \cdot \dfrac{\kappa}{\kappa+1}\right)^{1/2} \cdot \left(\dfrac{2}{\kappa+1}\right)^{1/(k-1)} & for \quad \overline{P} < \overline{P}_{choke} = \left(\dfrac{2}{\kappa+1}\right)^{k/(k-1)} \\ \alpha' \cdot \left(2 \cdot \dfrac{\kappa}{\kappa-1}\right)^{1/2} \cdot \overline{P}^{1/k} \cdot \left(1 - \overline{P}^{k-1/k}\right)^{1/2} & for \quad \overline{P} > \overline{P}_{choke} \end{cases} \quad (4)$$

where κ is the gas specific heat ratio, and (α') is a non-isentropic loss coefficient. Thus, the flow restriction is of inherent type with flow control strongly affected by the local film thickness.

An applied external static load (W_o) determines the rotor equilibrium position (e_X, e_Y)$_o$ with steady pressure field P_o and film thickness h_o, and corresponding pad deflections (δ_P, ξ_P, η_P)$_{o,\ P=1,\ldots Npad}$. Let the journal whirl with frequency ω and small amplitude motions (Δe_X, Δe_Y) about the equilibrium position. The general motion of the rotor center and pads is expressed as,

$$e_X = e_{Xo} + \Delta e_X\, e^{i\omega t}, \quad e_Y = e_{Yo} + \Delta e_Y\, e^{i\omega t}, \quad \xi_p = \xi_{po} + \Delta\xi_p\, e^{i\omega t}, \ i=(1)^{1/2}$$
$$\eta_p = \eta_{po} + \Delta\eta_p\, e^{i\omega t}, \quad \delta_p = \delta_{po} + \Delta\delta_p\, e^{i\omega t} \qquad p = 1,2,\ldots,N_{pad} \quad (5)$$

The film thickness and hydrodynamic pressure are also given by the superposition of equilibrium (zeroth order) and perturbed (first-order) fields, i.e.

$$h = h_o + \Delta h\, e^{i\omega t} \quad ; \quad P = P_o + \Delta P\, e^{i\omega t} \quad (6)$$

where $$\Delta h = \Delta e_X \cos\theta + \Delta e_Y \sin\theta + \Delta\xi_P \cos(\theta - \Theta_P) + (\Delta\eta_P - R\,\Delta\delta_P)\sin(\theta - \Theta_P) \quad (7)$$

and $$\Delta P = \{ P_X\, \Delta e_X + P_Y\, \Delta e_Y + P_\delta\, \Delta\delta_P + P_\xi\, \Delta\xi_P + P_\eta\, \Delta\eta_P \} \quad (8)$$

Substitution of (6) into the Reynolds equation (2) leads to a nonlinear PDE for the equilibrium pressure (P_o) and five linear PDEs for the first-order fields. Solution of the equations determines the pressure fields for calculation of the bearing reaction loads and moments as well as the stiffness and damping coefficients, $(K_{\alpha\beta}\ ,\ C_{\alpha\beta})_{\ \alpha\beta=X,Y}$. These force coefficients, relating radial forces to journal displacements, are of utmost importance in rotordynamic analysis, i.e.

$$\begin{bmatrix} F_X \\ F_Y \end{bmatrix} = -\begin{bmatrix} K_{XX} & K_{XY} \\ K_{YX} & K_{YY} \end{bmatrix}\begin{bmatrix} X \\ Y \end{bmatrix} - \begin{bmatrix} C_{XX} & C_{XY} \\ C_{YX} & C_{YY} \end{bmatrix}\begin{bmatrix} \dot{X} \\ \dot{Y} \end{bmatrix} \tag{9}$$

An iterative procedure based on the Newton-Raphson method is easily implemented for simultaneous satisfaction of the overall load balance, and the forces and moment balance on each pad. The method was introduced in [12] for the analysis of flexure pivot tilting pad hydrodynamic bearings. The numerically stable method of solution follows the exact procedure given in [17]. The method avoids spurious numerical oscillations and allows prediction of gas film static and dynamic characteristics for arbitrarily high-speed gas bearing numbers.

3. DESCRIPTION OF TEST RIG AND BEARINGS

Figure 3 depicts the test rig with a steel main body integrating a brushless electric motor armature (top speed 100 krpm). The motor drives a rotor supported on two identical flexure pivot pad gas bearings. See Table 1 for the bearing geometry and operating characteristics. References [1-4] detail the test rig components, AC motor integral to the rotating shaft, and the design and operating envelope of the test bearings.

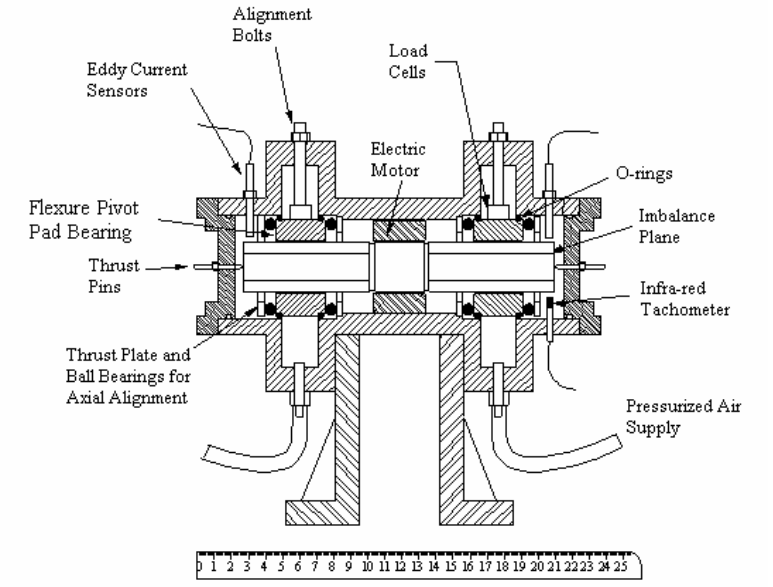

Figure 3. Schematic cross section view of gas bearing test rig (Unit: cm)

Pairs of eddy current sensors, orthogonally positioned and facing the rotor ends, record the shaft motions along the *X-(*vertical*)* and *Y-(*horizontal*)* directions. Three piezoelectric load cells, 120 ° apart, are connected to each bearing for measurement of the transmitted load. Positioning bolts secure the load cells and bearing in place. Zhu and San Andrés[3] describe the coast-down speed tests to record the rotor motions and transmitted bearing loads for various imbalance conditions and three feed absolute pressures, 2.4, 3.8 and 5.1 bars (20, 40 and 60 psig). The imbalance responses show the supply pressure raising the system critical speed (increase in bearing direct stiffness) while the viscous damping ratio decreases.

Parameter	Value	Unit
Rotor mass, M	0.827	kg
Rotor diameter with coating, D_J	28.50 ± 0.001	mm
Bearing bore diameter, D	28.58 ± 0.003	mm
Bearing clearance, C_p	40 ± 4.5	μm
Bearing axial length, L	33.2	mm
Pads number and arc length	4 (72 °)	Offset 60%
Pad preload, r_P	14	μm
Pad mass moment of inertia, I_P	0.253	gram-mm^2
Web rotational stiffness, $K_{\delta\delta}$	20	Nm/rad
Feed orifice diameter	0.62	mm
Operating conditions:		
Gas Constant, R_g	286.7 J/Kg-ºC (air)	
Temperature, T	27 ºC	
Viscosity, μ	1.85x 10^{-6} Pa-s	
Density, ρ_a	1.16 kg/m^3	
Ambient pressure, P_a	1.01 bar	

Table 1. Dimensions of test flexure pivot - tilting pad bearing and rotor

4. PREDICTIONS FROM GAS FILM MODEL AND COMPARISONS TO TEST RESULTS

Mass flow rate Figure 4 depicts the measured and predicted mass flow rate through each test bearing for increasing supply pressures, 1 to 5 bar. The computed results agree very well with the measurements, demonstrating the accuracy of the inherent orifice flow model. Note that even for the highest feed pressure, the predicted film pressure is not low enough to cause flow choking.

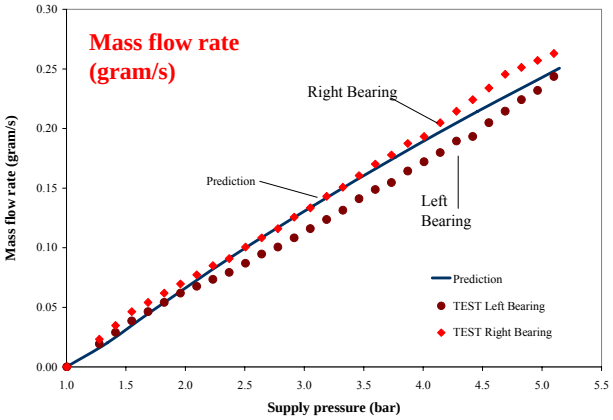

Figure 4. Bearing flow rate vs feed pressure. Measurements [3] and predictions. Rotor speed: 10 to 60 krpm

Stiffness coefficients Direct force coefficients, stiffness and damping, synchronous with shaft speed, were identified in [3] from measurements of the shaft displacements and transmitted loads to the rig casing. The identification procedure uses the synchronous components of rotor motion and loads, and relies heavily on the accurate measurement of the phase angle. Large uncertainties are expected while the rotor passes through the critical speed since the rotor/bearing system had very little damping.

Figure 5 shows the direct stiffnesses, K_{XX}, versus rotor speed for three test pressures. Predictions are depicted for identical pressures and the hydrodynamic condition. Note that the model predictions correctly show the trend of increasing direct stiffness as the shaft speed increases. The best correlation between test results and predictions is for a supply pressure of 2.36 bar (20 psig).

Figure 6 depicts the test derived and predicted direct damping coefficients, C_{YY}, versus rotor speed. The model damping values are still larger than the identified parameters; however, the trend in reduction in viscous damping as the feed pressure increases is correct.

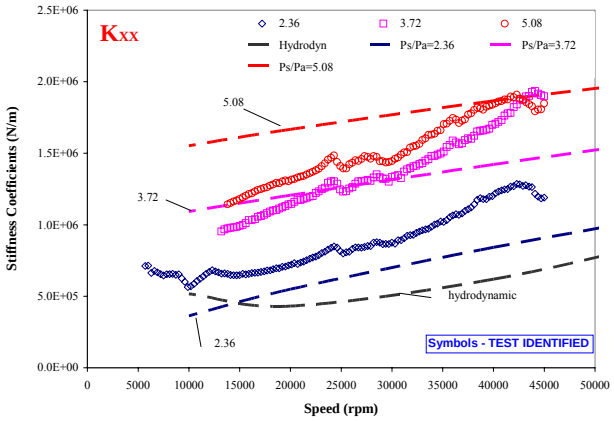

Figure 5. Bearing direct stiffness coefficient (K_{XX}) vs rotor speed for three magnitudes of gas supply pressure. Comparison of predictions to identified synchronous force coefficients from measurements

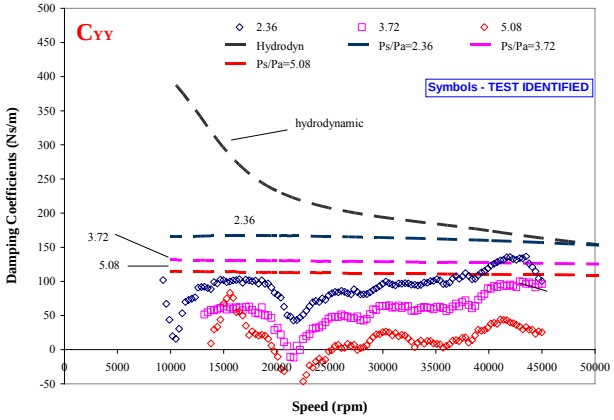

Figure 6. Bearing direct damping coefficient (C_{YY}) vs rotor speed for three magnitudes of gas supply pressure. Comparison of predictions to identified synchronous force coefficients from measurements

Coastdown rotor speed Once a rotor lifts on its gas bearings, the drag friction is very small since air has very low viscosity. This is obviously one of the major advantages of gas bearings. Figure 7 shows the recorded coast down speed of the test rotor versus time. Note the large time, well over 2 minutes, for the rotor to decelerate to rest from a top speed of 60 krpm. Note that increasing the feed pressure tends to increase the overall time of rotor lift off, in particular at very low shaft speeds.

The test data shows that the decay of shaft speed is of exponential type, i.e. due solely to viscous drag effects, for most of the operating speed range. Thus, a simple model of the form, $\Omega = \Omega_o\, e^{-t/\tau}$, $\tau = I_p/(2\, C_{\theta\theta})$, where τ is the system time constant and $C_{\theta\theta}$ is a rotational viscous damping coefficient derived from the drag torque in the bearings ($C_{\theta\theta} = T_{orque}/\Omega$) and windage effects from the motor armature. The experimental time constant for the system ranges from 63 s to 57 s as the supply pressure decreases (average value 60.3 s), while the estimation derived from predictions of the drag torque from the bearings (alone) equals 89 s. The difference is certainly due to the not quantified drag in the motor. The time constant estimation serves to validate indirectly the prediction of the drag torque in the bearings.

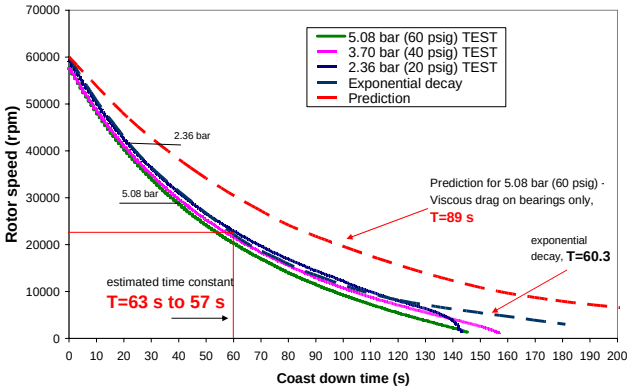

Figure 7. Recorded coast down rotor speed vs time for three feed pressures (2.36, 3.70 and 5.08 bar).

Predictions of rotordynamic response A FE structural model for the test rotor was developed using an in-house rotordynamics software tool. The model replicates very well the free-free elastic modes of the composite rotor and verifies this is nearly rigid within the range of operating shaft speeds, maximum 100 krpm. The predicted synchronous force coefficients for each pressure condition are incorporated into the program for prediction of the rotor imbalance response. Note that gas bearings have frequency dependent force coefficients which must be used in system eigenvalue analysis determining the natural frequencies and damping ratios for stable performance.

Figure 8 presents the predicted and measured synchronous rotor response for a condition of feed pressure equal to 2.36 bar (20 psig). The correlation of linear rotordynamic predictions to the test data is remarkable. The figure includes the imbalance masses used in the analysis. The actual imbalance is unknown. The one used was determined from matching the peak amplitude of motion at the critical speed.

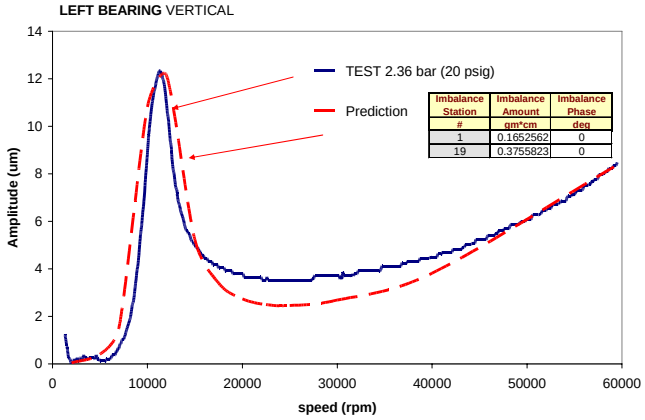

Figure 8 Comparison of predicted and measured imbalance response for supply pressure 2.36 bar (20 psig). Left Bearing, vertical plane. Mass imbalances noted

5. CONCLUSIONS

To date the hybrid flexure pivot-tilting pad bearings (FPTPBs) have demonstrated superior static and dynamic forced performance than simple three-lobe bearings and Rayleigh-step bearings. The FPTPBs are mechanically complex and more expensive; however, their enhanced stability characteristics and predictable rotordynamic performance, with verified operation to speeds as high as 100 krpm, makes them desirable for the envisioned oil-free applications in high speed micro turbomachinery.

A computational model including the effects of external pressurization predicts the rotordynamic coefficients of the test bearings and shows good correlation with measured force coefficients, thus lending credence to the

predictive model. In general, direct stiffnesses increase with operating speed and external pressurization; while damping coefficients show an opposite behavior. The rotational structural stiffness of the pad web determines the amount of cross-coupled stiffness coefficients in a FPTPB. Correlation of predicted mass flow rates and measurements also validates the inherent orifice-flow model. Finally, predictions of the drag torque from the gas bearings also verify indirectly the test measurements which show very long times for coasting down; thus demonstrating a nearly friction-free operation.

6. ACKNOWLEDGMENTS

This material is based upon work supported by the National Science Foundation under Grant No. 0322925. The support of the TAMU Turbomachinery Research Consortium is also acknowledged.

7. REFERENCES

[1] Wilde, D.A., and San Andrés, L., 2003, "Experimental Response of Simple Gas Hybrid Bearings for Oil-Free Turbomachinery," ASME Paper GT 2003-38833.

[2] Wilde, D.A., and San Andrés, L., 2003, "Comparison of Rotordynamic Analysis Predictions with the Test Response of Simple Gas Hybrid Bearings for Oil Free Turbomachinery," ASME Paper GT2003-38859.

[3] Zhu, S. and L., San Andrés, 2004, "Rotordynamic Performance of Flexure Pivot Hydrostatic Gas Bearings for Oil-Free Turbomachinery," ASME Paper GT 2004-53621.

[4] Zhu, S. and L., San Andrés, 2005, "Experimental response of a Rotor Supported on Rayleigh Step Gas Bearings, ASME Paper GT2005-68296.

[5] Lund, J. W., 1967, "A Theoretical Analysis of Whirl Instability and Pneumatic Hammer for a Rigid Rotor in Pressurized Gas Journal Bearings", ASME Journal of Lubrication Technology, Vol. 89, pp. 154-163.

[6] Stowell, T. B., 1971, "Pneumatic Hammer in a Gas Lubricated Externally Pressurized Annular Thrust Bearing", ASME Journal of Lubrication Technology, Vol. 93, pp. 498-503.

[6] Wong, R. Y., Stewart, W. L., and Rohlok, H. E., 1968, "Pivot-Pad Journal Gas Bearing Performance in Exploratory Operation of Brayton Cycle Turbocompressor", ASME Journal of Lubrication Technology, Vol. 90, pp. 687-700.

[7] Lund, J. W., and Pederson, L. B., 1987, "The Influence of Pad Flexibility on the Dynamic Coefficients of a Tilting Pad Journal Bearing", ASME Journal of Lubrication Technology, Vol. 109, pp. 65-70.

[8] Zeidan, F.Y., 1992, "Developments in Fluid Film Bearing Technology," Turbomachinery International, pp. 24-31.

[9] Armentrout, R. W., and Paquette, D. J., 1993, "Rotordynamic Characteristics of Flexure-Pivot Tilting-Pad Journal Bearings", STLE Tribology Transactions, Vol. 36, pp. 443-451.

[10] Chen, W. J., Zeidan, F. Y., and Jain, D., 1994, "Design, Analysis and Testing of High Performance Bearing in a High Speed Integrally Geared Compressor", Proceeding of the 23rd Turbomachinery Symposium, pp. 31-42.

[11] Chen, W.J., 1995, "Bearing Dynamic Coefficients of Flexible-Pad Journal Bearings," STLE Transactions, 38(2), pp. 253-260.

[12] San Andrés, L., 1996, "Turbulent Flow, Flexure-Pivot Hybrid Bearings for Cryogenic Applications," ASME Journal of Tribology, Vol. 118, 1, pp. 190-200.

[13] Czolczynski, K., 1999, "Rotordynamics of Gas-Lubricated Journal Bearing System", Springer Verlag.

[14] San Andrés, L. and D., Wilde, 2001, "Finite Element Analysis of Gas Bearings for Oil-Free Turbomachinery," Revue Européenne des Eléments Finis, Vol. 10 (6/7), pp. 769-790.

[15] Delgado, A., L., San Andrés, and J. Justak, 2004, "Analysis of Performance and Rotordynamic Force Coefficients of Brush Seals with Reverse Rotation Ability", ASME Paper GT 2004-53614.

[16] Mori, H., and Miyamatsu, Y., 1969, "Theoretical Flow-Models for Externally Pressurized Gas Bearings", ASME Journal of Lubrication Technology, Vol. 91, pp. 183-193.

[17] Faria, M., and L. San Andrés, 2000, "On the Numerical Modeling of High Speed Hydrodynamic Gas Bearings," ASME Journal of Tribology, Vol. 122, 1, pp. 124-130.